

Mitigating Interfacial Mismatch between Lithium Metal and Garnet-Type Solid Electrolyte by Depositing Metal Nitride Lithiophilic Interlayer

Abiral Baniya, Ashim Gurung, Jyotshna Pokharel, Ke Chen, Rajesh Pathak, Buddhi Sagar Lamsal, Nabin Ghimire, Raja Sekhar Bobba, Sheikh Ifatur Rahman, Sally Mabrouk, Alevtina L. Smirnova, Kang Xu, and Quinn Qiao*



Cite This: *ACS Appl. Energy Mater.* 2022, 5, 648–657



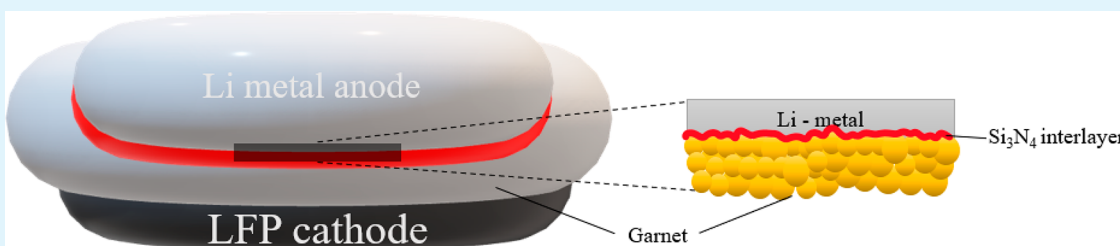
Read Online

ACCESS |

Metrics & More

Article Recommendations

Supporting Information



ABSTRACT: Solid-state lithium batteries are generally considered as the next-generation battery technology that benefits from inherent nonflammable solid electrolytes and safe harnessing of high-capacity lithium metal. Among various solid-electrolyte candidates, cubic garnet-type $\text{Li}_7\text{La}_3\text{Zr}_2\text{O}_{12}$ ceramics hold superiority due to their high ionic conductivity (10^{-3} to 10^{-4} S cm $^{-1}$) and good chemical stability against lithium metal. However, practical deployment of solid-state batteries based on such garnet-type materials has been constrained by poor interfacing between lithium and garnet that displays high impedance and uneven current distribution. Herein, we propose a facile and effective strategy to significantly reduce this interfacial mismatch by modifying the surface of such garnet-type solid electrolyte with a thin layer of silicon nitride (Si_3N_4). This interfacial layer ensures an intimate contact with lithium due to its lithiophilic nature and formation of an intermediate lithium–metal alloy. The interfacial resistance experiences an exponential drop from 1197 to 84.5 Ω cm 2 . Lithium symmetrical cells with Si_3N_4 -modified garnet exhibited low overpotential and long-term stable plating/stripping cycles at room temperature compared to bare garnet. Furthermore, a hybrid solid-state battery with Si_3N_4 -modified garnet sandwiched between lithium metal anode and LiFePO_4 cathode was demonstrated to operate with high cycling efficiency, excellent rate capability, and good electrochemical stability. This work represents a significant advancement toward use of garnet solid electrolytes in lithium metal batteries for the next-generation energy storage devices.

KEYWORDS: solid-state electrolytes, lithium/garnet interface, interfacial resistance, solid-state batteries, silicon nitride

1. INTRODUCTION

Currently, lithium-ion batteries (LIBs) are used worldwide as the workhorse for powering applications.^{1,2} The ceiling of energy density allowed by commercial intercalation chemistries approaches 300 Wh/kg, while any attempt to push the energy density higher must face the risks imposed by highly flammable organic electrolyte solvents. Replacing graphite with lithium metal (Li^0) as anode presents an ultimate solution, since lithium combines high specific capacity (3860 mAh g $^{-1}$) with the lowest reduction potential (-3.04 V vs Li/Li $^+$) among all elements in the Periodic Table.³ However, such low potential also makes lithium extremely reactive when in contact with almost any liquid electrolyte component. Liquid electrolytes also impose limitations on performance of high-voltage cathodes, due to their lower anodic stability.⁴ Therefore, development of high-energy and safe battery technologies

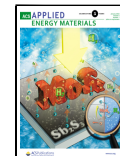
relies on the replacement of liquid electrolytes with a fast ion conductor that does not combust. Solid-state batteries (SSBs) employing solid-state electrolytes (SSEs) hold such promises for the next-generation energy storage devices as long as they could be stable in the presence of both lithium and high-voltage cathode while conducting ions at fast rate.^{5,6}

Several solid-electrolyte systems have been thoroughly explored, which range from sulfides to oxides and oxynitrides such as perovskite,⁷ antiperovskite,⁸ LISICON,⁹ thio-LISI-

Received: October 8, 2021

Accepted: December 22, 2021

Published: January 7, 2022



CON,¹⁰ NASICON,¹¹ garnet,¹² sulfide glass ceramic,^{13–15} etc. Certain sulfide SSEs (e.g., LGPS) are known for their ionic conductivity above 1 mS cm^{−1} at room temperature, but their sulfide nature renders them to be thermodynamically unstable against Li⁰ or high-voltage cathodes,^{16–19} while electrolytes, such as LIPON^{20,21} and LATP,^{22,23} also tend to react with Li⁰ anode (e.g., Ti⁴⁺/Ti³⁺ redox reaction). Only garnet SSEs, represented by Li₇La₃Zr₂O₁₂ (LLZO), provides high ionic conductivity close to 1 mS cm^{−1} at room temperature, a wide electrochemical window, and good electrochemical stability against Li⁰ anode.^{24,25}

However, a major hurdle for garnets still exists: its poor contact with Li⁰, which arises from the microscopic gaps that are prevalent at solid–solid interfaces, and always leads to high interfacial impedance and poor cycling performance. Diversified strategies²⁶ such as altering the chemical composition of the electrolyte,²⁷ applying external heat and pressure,²⁸ electrolyte surface modification,²⁹ and interface modification³⁰ have been adopted, among which the introduction of a buffer layer between garnet SSEs and Li⁰ has been proven efficient and promising. Buffer layers in the form of metals (such as Au,³¹ Al,³² Si,³³ Ge,³⁴ Mg³⁵), metal oxides (such as Al₂O₃,³⁶ ZnO³⁷), and carbon material (such as graphite³⁸) have significantly reduced impedance and improved cell performances. Computational analysis has revealed that material stability against Li⁰ depends on their cation and anion chemistry.³⁹ Upon contact with Li⁰ these oxides, sulfides, and fluorides usually become unstable, which leads to the formation of an interlayer that consumes active materials and serves as a physical barrier to ion transport. Hence, metal nitrides are preferred as they are more stable against Li⁰ than oxides, sulfides, and fluorides.³⁹

Here, we report a novel nitride interface modifier by coating the garnet-type Li_{6.25}Al_{0.25}La₃Zr₂O₁₂ (Al-LLZO) solid electrolyte with a thin layer of Si₃N₄ deposited by radio frequency (RF) sputtering technique. This interfacial buffer layer enabled establishment of a homogeneous and intimate physical contact between the SSE and Li⁰. Thus, the developed nitride interface, denoted as Si₃N₄@Al-LLZO, showed a stable interface during cycling of symmetrical cells for a prolonged period of more than 800 h. With optimization of the Si₃N₄@Al-LLZO interfacial layer, Li/Si₃N₄@Al-LLZO/LFP full cells showed excellent overall cycling and rate performance.

2. EXPERIMENTAL SECTION

2.1. Garnet Al-LLZO Solid-Electrolyte Pellets Preparation.

A 0.4 g amount of cubic phase aluminum doped lithium lanthanum zirconate garnet nanopowder, Li_{6.25}Al_{0.25}La₃Zr₂O₁₂ (Ampcera Inc., 99.9%), was pressed into pellet by using 1/2 in. dry pellet pressing die (MTI Corp.) and applying 80 MPa pressure using a hydraulic laboratory press (Carver Inc.). Thus, obtained pellets were carefully placed on a magnesium oxide (MgO) crucible, covered with same mother powder and sintered in a furnace (Mellen, Microtherm) at 1280 °C for 1 h. After the pellets were left to cool to room temperature, they were dry polished from 1000, 1500, and 2000 to 3000 grit sized sandpapers using a rotary tool set (Fire Mountain Gems and Beads, USA). The polished pellets were stored in an argon glovebox for future use.

2.2. Si₃N₄ Interfacial Layer Deposition.

Thin films of Si₃N₄ were deposited on polished Al-LLZO pellets using RF sputtering. A 2 in. diameter × 0.125 in. thick, 99.9% metals basis, silicon(IV) nitride (Si₃N₄) sample with MgO binder (Alfa Aesar) was used as target. The sputtering process was carried out at a deposition rate of 0.1 Å s^{−1} with 50 sccm constant flow of argon (Ar) gas. Various thicknesses

(20, 30, and 40 nm) of Si₃N₄ thin films were investigated, and the thickness was optimized to 30 nm.

2.3. Solid-State Lithium Symmetrical Cells and Hybrid Solid-State Full Cells Assembly. First, for analyzing the ionic conductivity and cycling stability of as-prepared solid electrolytes, Li/Si₃N₄/Al-LLZO/Si₃N₄/Li symmetric cells were prepared by attaching the melted Li at 200 °C on both sides of the electrolyte pellets. After natural cooling, the Li/Si₃N₄/Al-LLZO/Si₃N₄/Li sample was assembled into coin cells in an argon-filled glovebox. Control symmetric cells without interface modification were also assembled for comparison with the modified one. Second, for preparation of Li/Si₃N₄@Al-LLZO/LFP hybrid solid-state full cells, the as-prepared Li/Si₃N₄@Al-LLZO sample was assembled with LiFePO₄ (LFP) as cathode in a coin cell. For this, the cathode slurry was prepared by mixing LFP powders with Super-P carbon black and poly(vinylidene fluoride) (PVDF) at the weight ratio of 80:10:10, respectively, in N-methyl-2-pyrrolidone (NMP) solvent, using mortar and pestle. The as-prepared slurry was coated onto an aluminum foil and then dried in a vacuum oven at 120 °C overnight for thorough evaporation of the solvent. The dried cathode strips were then punched into circular disks with the active materials mass loading of ~2 mg cm^{−2}. Lastly, for assembly of hybrid solid-state full cell a tiny amount of 10 μL of liquid electrolyte (1.0 mol L^{−1} LiPF₆ dissolved in ethylene carbonate (EC) and diethyl carbonate (DEC) in volume ratio of 1:1) was introduced between LFP cathode and solid-electrolyte pellet to enhance the cathode/electrolyte interface contact. The other side of the Al-LLZO pellet with no trace of liquid electrolyte was modified by Si₃N₄ deposition, and melted lithium was soldered on the top of it. The assembled full cell was sealed in a 2032 coin cell with nickel foam on the top for absorbing the excess pressure during crimping and avoiding damage to the solid-electrolyte pellet. The assembly of symmetric cells and full cells was done inside an argon-filled glovebox with moisture and O₂ levels < 1 ppm.

2.4. Material Characterizations. The crystal structure of the samples was examined by X-ray diffraction (XRD) using a Rigaku SmartLab diffractometer with Cu K α radiation ($\lambda = 1.54178$ Å). Surface topography of bare garnet and Si₃N₄-modified garnet pellets were measured by an Agilent SPM 5500 atomic force microscope that is equipped with a MACIII controller and a RTESPA-525 tip with resonance frequency of 75 kHz. To observe the morphology of the samples, scanning electron microscopy (SEM) characterization was carried out using a Hitachi S-4300N scanning electron microscope, which was also equipped with energy-dispersive spectroscopy (EDS). Electrochemical impedance spectroscopy (EIS) measurement was done using the Ametek VERSASTAT3-200 potentiostat electrochemical workstation. The measurement was performed over a working frequency range of 1 MHz to 100 mHz with an amplitude of 10 mV. To measure the ionic conductivity of an Al-LLZO garnet-type pellet, 20 nm of gold (Au) layers were sputtered on both sides of the pellet as blocking electrode. Galvanostatic charge/discharge measurements of assembled coin cells were performed using a LAND CT2001A system. The full cells were cycled at various current densities (e.g., 1C = 170 mA g^{−1}) in a voltage range of 4.0 to 2.5 V. The coin cells were tested at room temperature.

3. RESULTS AND DISCUSSION

3.1. Structure, Composition, and Kinetics of Prepared SSE.

The cubic phase Li_{6.25}Al_{0.25}La₃Zr₂O₁₂ garnet nanopowder was pressed, sintered, and polished into solid-electrolyte pellets (Supporting Information Figure S1). As shown in Figure S2c, first, XRD was performed on a polished pellet, pressed using as-received Al-LLZO powder and sintered at 1000 °C. The impurity peaks, marked with an asterisk (*), were identified as La₂Zr₂O₇ (PDF No. 50-0837). Further, when the garnet nanopowder was pressed, sintered (>1200 °C), and polished, most of the impurity peaks of La₂Zr₂O₇ disappeared and the one at about 29° was much suppressed, marked by a red diamond, which indicated formation of a rather pure cubic

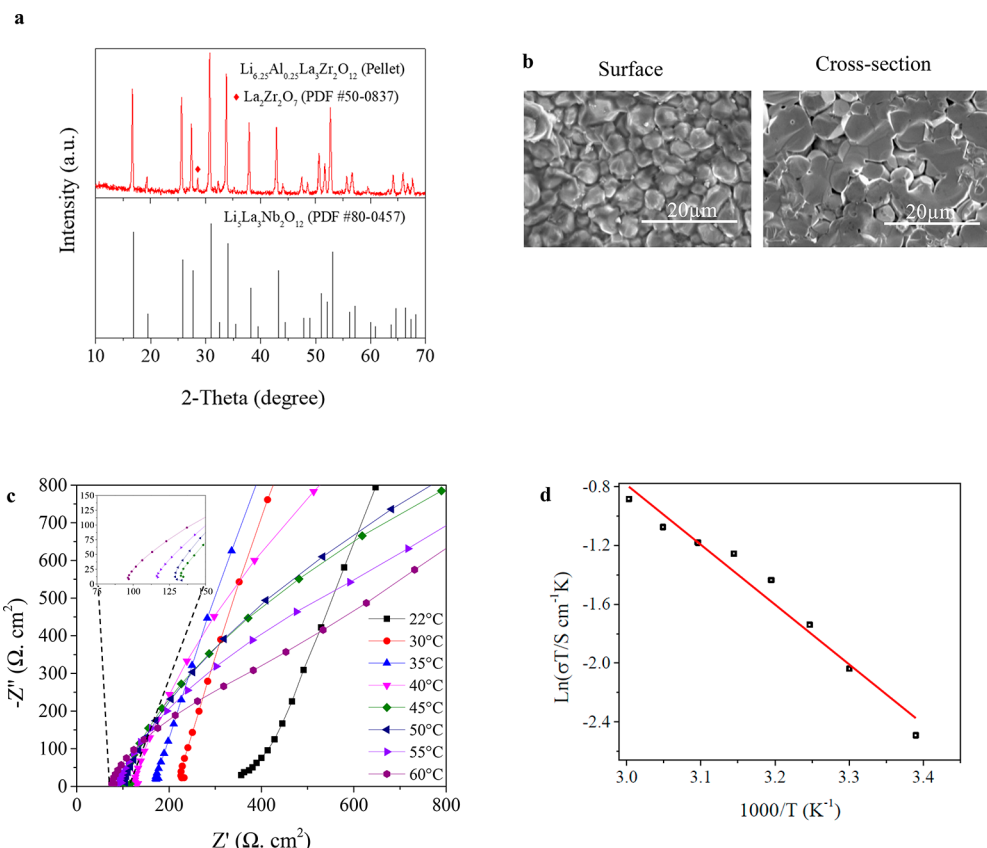


Figure 1. Characterization of as-prepared Al-LLZO garnet electrolyte pellet. (a) XRD comparison of Al-LLZO garnet pellet that matches with cubic structure $\text{Li}_5\text{La}_2\text{Nb}_2\text{O}_{12}$. (b) Surface and cross-section SEM images of Al-LLZO pellets. (c) EIS spectra of Al-LLZO electrolyte at elevated temperatures ranging from 22 to 60 °C. Inset showing spectra from 45 to 60 °C. (d) Arrhenius plot of Al-LLZO ionic conductivity.

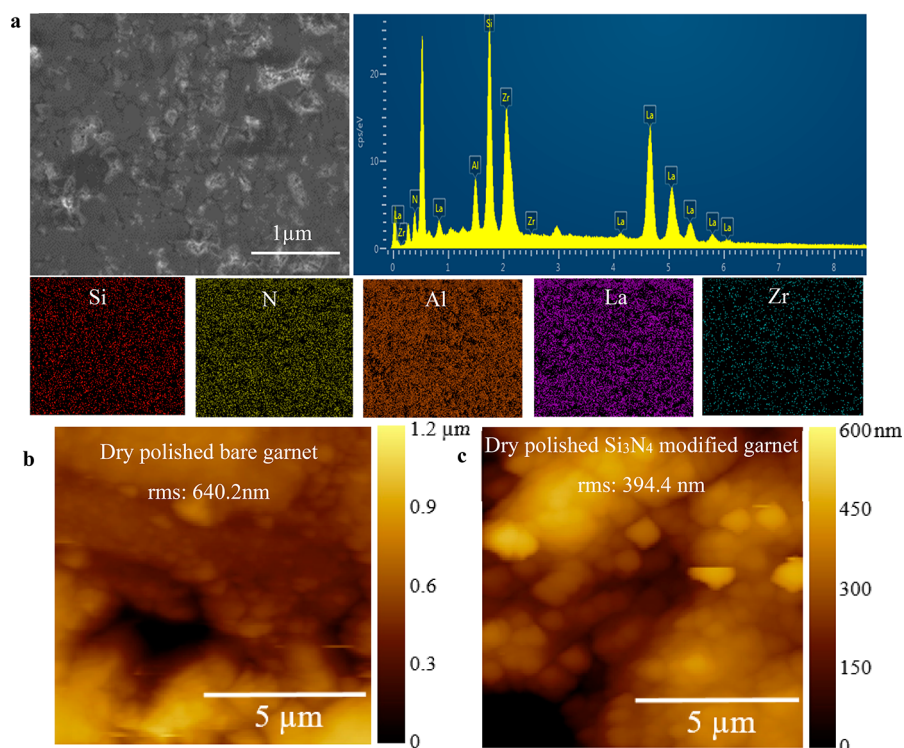


Figure 2. EDS spectrum and AFM mapping of bare and Si_3N_4 -modified Al-LLZO garnet pellet SSE surface. (a) EDS spectrum shows presence of Si and N along with elements from SSE. AFM topography mapping of dry polished (b) bare garnet and (c) Si_3N_4 -modified garnet.

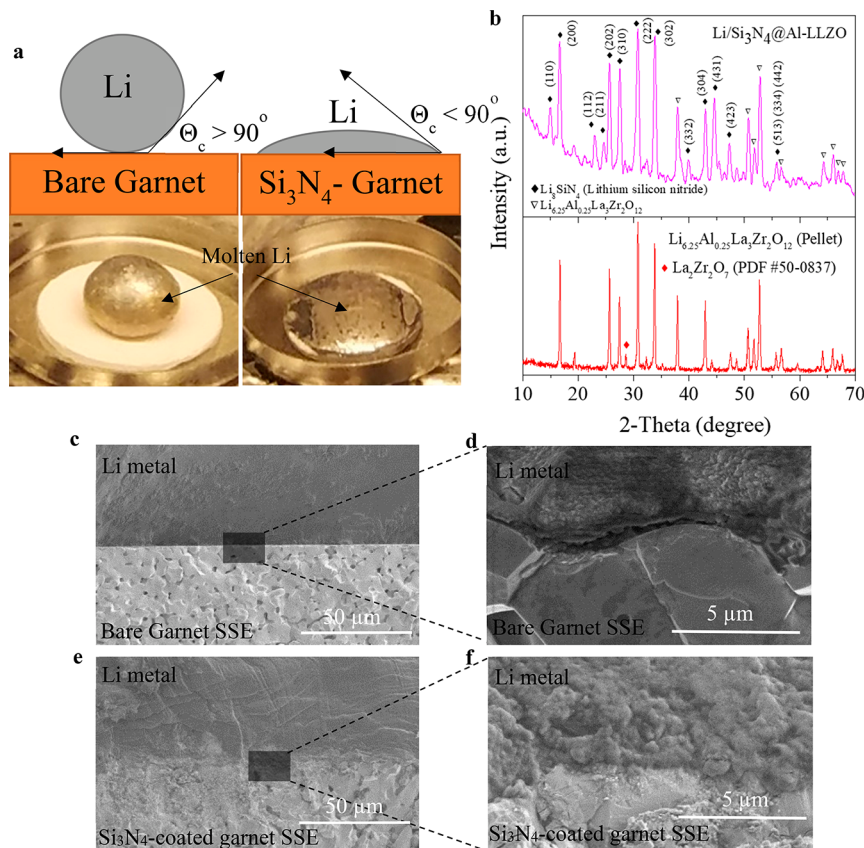


Figure 3. Wetting behavior and interfacial contact characterization of Li/Li₃N₄-coated garnet SSE. (a) Digital images of bare Al-LLZO garnet pellet with molten Li on top with contact angle ($\theta_c > 90^\circ$), and Si₃N₄-deposited Al-LLZO pellet with molten Li on top with contact angle ($\theta_c < 90^\circ$). (b) XRD comparison of thus prepared bare garnet and Si₃N₄-coated garnet. Cross-section SEM images of Li/Al-LLZO interface (c, d) without and (e, f) with a Si₃N₄ interlayer.

phase Al-LLZO garnet pellet. Also, XRD patterns (Figure 1a) of as-prepared solid-electrolyte pellets show the resemblance of diffraction peaks when indexed to the standard pattern of cubic garnet phase Li₅La₃Nb₂O₁₂ (PDF No. 80-0457). Further, the surface and cross-section SEM images (Figure 1b) show well-densified pellets with the majority of grains tightly connected when sintered at 1280 °C for an hour. These sintered pellets have relative densities of ~92% (Figure S2) when measured using Archimedes' principle and ethanol as immersion medium.⁴⁰

The ionic conductivities of Al-LLZO pellets were evaluated using EIS with Au layers as blocking electrodes. The total Li-ion conductivity of Al-LLZO pellets using the low-frequency intercept value was calculated to be 2.81×10^{-4} S cm⁻¹. The Li-ion conductivity of Al-LLZO was also measured at temperatures ranging from 22 to 65 °C (Figure 1c), where the low-frequency intercept value decreases (Figure S3c) by following typical Arrhenius behavior (Figure 1d). Activation energy (E_a) for Li-ion conduction was calculated using eq 1:

$$\sigma = \frac{A}{T} \exp\left(\frac{-E_a}{k_b T}\right) \quad (1)$$

where A is a pre-exponential factor, E_a is the activation energy, k_b is the Boltzmann constant, and T is the absolute temperature. Thus, observed activation energy and Li-ion conductivity of 0.34 eV and 2.81×10^{-4} S cm⁻¹ at 22 °C, respectively are in line with other reports for garnet SSE.^{41–43}

3.2. Metal Nitride Interface Layer Properties. The improved interfacial contact between Li⁰ and Al-LLZO garnet electrolyte is crucial for enhanced ion transport and even current distribution at the interface. However, the contact between Li⁰ and bare garnet consists of voids and gaps leading to uneven current distribution at the interface that accelerates dendrite or dead Li⁰ growth that could short circuit through the solid electrolyte. To address this issue, a thin film of Si₃N₄ was sputter deposited on top of an Al-LLZO garnet pellet. Figure 2a shows the energy-dispersive X-ray spectroscopy (EDS) spectrum and mapping of a Si₃N₄-deposited Al-LLZO garnet pellet, which reveals the presence of La, Zr, and Al in the garnet along with N and Si attributed to the deposited Si₃N₄. Further, atomic force microscopy (AFM) performed on bare (Figure 2b) and Si₃N₄-modified (Figure 2c) garnet samples compares their surface roughness using the average surface root-mean-square (RMS) values, which reveals the presence of Si₃N₄ significantly reduces the RMS value from 640.2 nm of bare garnet to 394.4 nm. The higher RMS value represents the uneven and rough surface of dry polished bare garnet that leads to poor contacts⁴⁴ and induces uneven current distribution^{45,46} that eventually leads to preferential deposition of Li⁰⁴⁷ on certain spots and formation of dendrites.⁴⁸ The lower RMS value of Si₃N₄-modified dry polished garnet should result in much more uniform and stable Li plating/stripping that is conducive for longer cycling life.⁴⁹

After Si₃N₄ thin film deposition, as shown in SEM images of Figure 3e,f, the Li⁰ anode has been tightly soldered with an Al-LLZO pellet as no gaps and voids are visible in comparison to

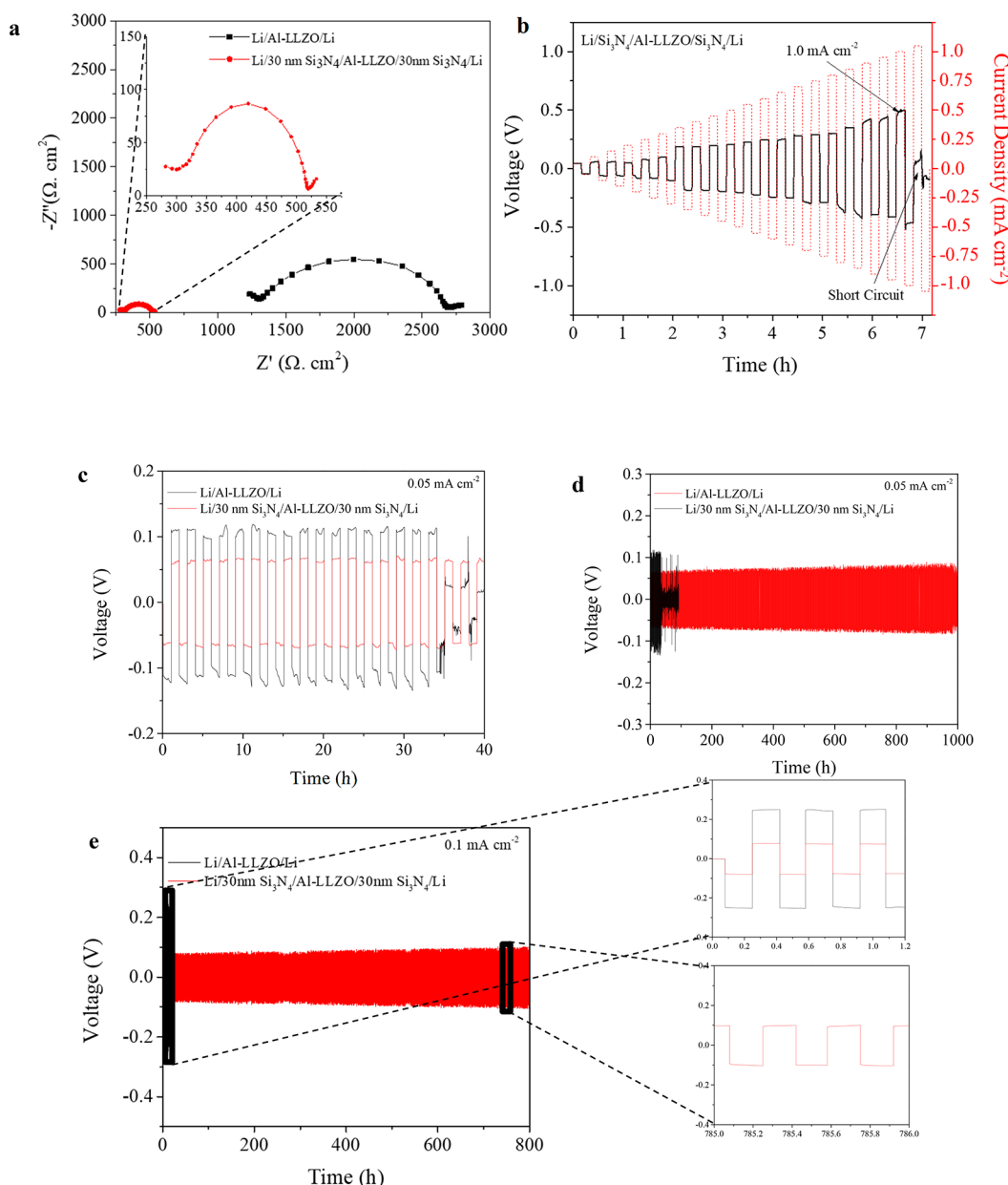


Figure 4. Electrochemical stability of interface-modified SSE. (a) Nyquist plots of Li symmetrical cells for Al-LLZO with and without Si_3N_4 modification. (b) Critical current density (CCD) plot for $\text{Li/Si}_3\text{N}_4/\text{Al-LLZO/Si}_3\text{N}_4/\text{Li}$ symmetric cell. Galvanostatic cycling performance of Li/Al-LLZO/Li symmetrical cells with and without Si_3N_4 modification at 0.05 mA cm^{-2} and 0.05 mAh cm^{-2} . (c) First few cycles and (d) long-term cycling. (e) Galvanostatic cycling performance of $\text{Li/Si}_3\text{N}_4/\text{Al-LLZO/Si}_3\text{N}_4/\text{Li}$ symmetric cell at constant current density of 0.1 mA cm^{-2} .

bare garnet (Figure 3c,d). This depicts that the Si_3N_4 thin film at the interface enabled the promotion of interfacial contact of Al-LLZO grains with lithium metal. To observe the lithiophilicity of the Si_3N_4 interfacial layer, a molten Li^0 droplet was applied to the bare and Si_3N_4 -coated garnet pellets, respectively. As observed from Figure 3a, the molten Li^0 on the top of the bare garnet pellet instantly beads up to form a ball, revealing its lithiophobicity. In contrast, with the Si_3N_4 -coated garnet, the molten lithium readily wets the surface and spreads out to fully cover it.

To further demonstrate this conversion of lithiophobicity to lithiophilicity, Li^0 foil was gradually heated on the top of the Si_3N_4 -coated garnet surface. As shown in Figure S4, when Li^0 starts to melt at $\sim 190^\circ\text{C}$, the Si_3N_4 -coated area in proximity to lithium metal turns black in color, which suggests occurrence

of lithiation reaction of as-deposited Si_3N_4 . This reaction not only occurred at the areas directly under lithium metal but also around the entire Si_3N_4 -coated garnet.

XRD was performed after Si_3N_4 deposition on an SSE pellet and infusing molten lithium on top of it. Figure 3b shows the appearance of some new peaks indicated as black-filled diamonds along with the common diffraction peaks related to Al-LLZO. These pronounced new peaks indicate the formation of tetragonal phase Li_8SiN_4 , lithium silicon nitride (JCPDS Card No. 40-1449)^{50,51} when lithium reacts with the silicon nitride layer at the interface and can also be verified from previous literature.⁵²⁻⁵⁹ The formation of ternary alloy phase Li_8SiN_4 is further explained in Figure 3b by identifying peaks using Miller indices. These peaks match the XRD data that are reported by Yamashita et al. in ref 60, by Yamane et al.

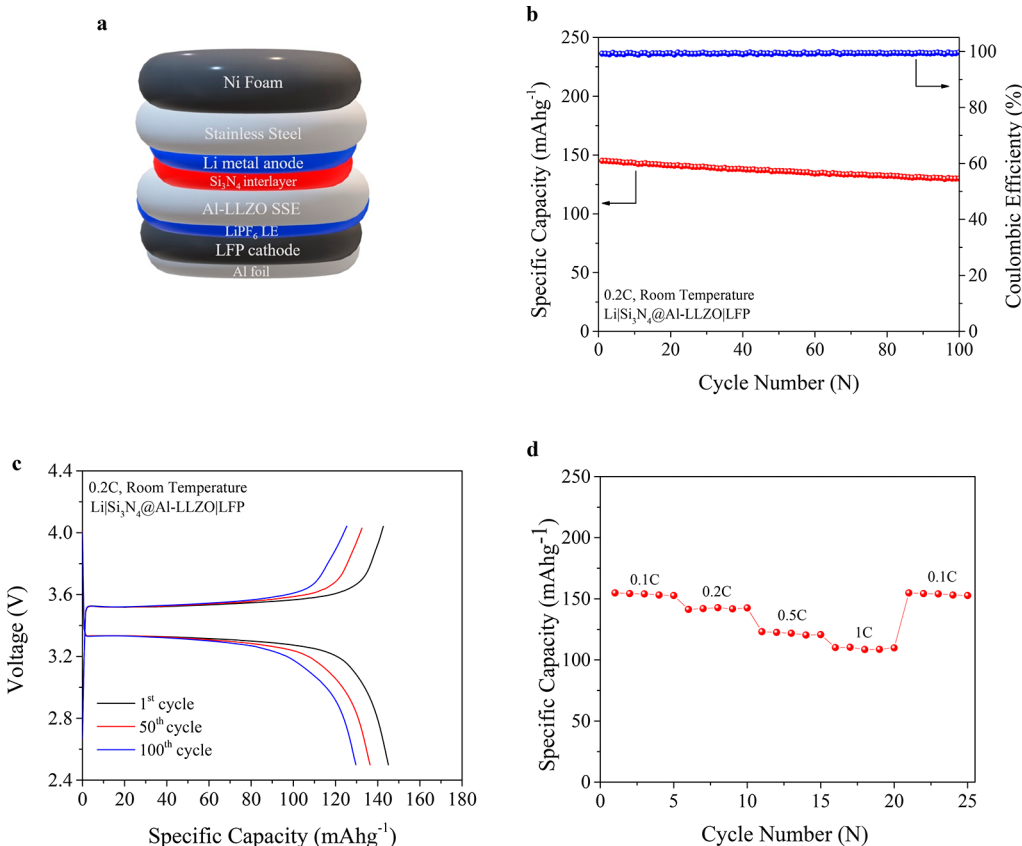
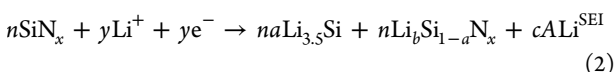


Figure 5. Full cell demonstration of electrochemical cells. (a) Schematic of device structure for Li/Si₃N₄@Al-LLZO/LFP cell. (b) Cycling performance of the cell at 0.2C-rate and room temperature. (c) Voltage profiles for selected cycles (first, 50th, and 100th) of Li/Si₃N₄@Al-LLZO/LFP cell at 0.2C and room temperature. (d) Rate performance of cell at different C-rates.

in ref 52, and from JCPDS Card No. 40-1449. These alloys at the interface provide open tunnels for Li⁺ conduction as all phases of these alloys are shown to conduct Li⁺ where a phase such as Li₈SiN₄ can show conductivity reaching as high as 5×10^{-2} S m⁻¹ at 400 K with lowest activation energy (46 kJ/mol).⁵² Studies by Yamane et al.⁵² and Ulvestad et al.⁵³ have shown the thermal formation of different ternary lithium silicon nitrides from Si₃N₄ when in contact with Li⁰. Heating was provided during infusion of molten Li⁰ in Si₃N₄ layer which further assists in formation of ternary phase alloy. These alloys are very ionically conductive, which is self-evident by the decrease in interfacial and charge transfer resistance by introduction of the Si₃N₄ interlayer. On the basis of this hypothesis, chemical eq 2 can best describe the initial reduction reaction:⁵³



Thus, the conversion reaction of Si₃N₄ film deposited at the interface with Li⁰³⁸ results in formation of ternary phase alloy, e.g., Li₈SiN₄,⁵² which enhances the interfacial contact.

Furthermore, coating amorphous silicon (Si) atoms have been known to switch the surface of garnet LLZO from “superlithiophobic” to “superlithiophilic”.⁵³ Similarly, lithium nitride (Li₃N) in cases of both garnet solid⁶¹ and carbonate based liquid electrolyte⁶² have been shown to drastically decrease the interfacial impedance and passivate the surface of Li anode. On the basis of these previous findings, silicon nitride (Si₃N₄) is propitious to show both strong wetting

interaction with molten Li⁰ due to the presence of nitride that undergoes alloying reaction.

3.3. Electrochemical Properties of Interface Stabilized SSE. Symmetric cells Li/Si₃N₄/Al-LLZO/Si₃N₄/Li and Li/Al-LLZO/Li were assembled and characterized, whose Nyquist plots (Figure 4a) show that the introduction of Si₃N₄ reduces total impedance (combined impedance of Al-LLZO electrolyte pellet and Li/Al-LLZO interface) from 2750 Ω cm² for the bare garnet to 525 Ω cm² for the modified one (Figure 4a). At 22 °C, the total impedance of the Au/Al-LLZO/Au sample was observed to be 356 Ω cm² (Figure 1c). Judging from the values from Figure 4a for combined impedances, the interfacial ASR has been reduced from 1197 to 84.5 Ω cm². Similarly, as shown in Figure 4b, the CCD of the Li/Si₃N₄/Al-LLZO/Si₃N₄/Li symmetric cell was tested and confirmed to be 1 mA cm⁻². This significant reduction of interfacial ASR can be attributed to (1) the Si₃N₄ interlayer promoting conformal contact of Li⁰ anode on SSE; (2) formation of thermally lithiated Si₃N₄ when Li⁰ is heated in contact with the interlayer; and (3) inhibition of impurity layers, such as, Li₂CO₃ due to coating of Si₃N₄ on SSE surface.

Galvanostatic Li plating/stripping cycling experiments using Li symmetrical cells were performed to assess the effectiveness of Li-ion transport across the interface and cycling stability. For this, various thicknesses of Si₃N₄ (for example 20, 30, and 40 nm) interlayer were deposited on top of the garnet surface and it was optimized to 30 nm (Figure S5). As shown in Figure 4 and Figure S6, plating/stripping cycles of symmetrical cells were performed in both low and high current densities of 0.05

and 0.2 mA cm^{-2} , respectively. Figure 4c shows comparison of the first few plating/stripping cycles of Li symmetrical cells based on bare garnet and Si_3N_4 -modified garnet cycled at current density of 0.05 mA cm^{-2} and capacity of 0.05 mAh cm^{-2} . It can be observed that the symmetric cell with bare garnet is plagued with large overpotential $> \pm 100 \text{ mV}$, while the cell with the Si_3N_4 interface layer facilitated the suppression of this overpotential to $\pm 60 \text{ mV}$. This indicates that the introduction of Si_3N_4 reduced the energy barrier of the lithium transfer process at the interface, thus facilitating the occurrence of efficient plating/stripping cycles. Longer plating/stripping cycling of these symmetrical cells was carried out as shown in Figure 4d. The cell with bare garnet short circuiting after only 35 h can be attributed to typical phenomenon of Li infiltration into SSE (Figure S6c).⁶³ In contrast, the cell with Si_3N_4 -modified garnet shows stable cycling for 1000 h, suggesting a stable interface enabled by Si_3N_4 thin film. Similar stable cycling up to 800 h at current density of 0.1 mA cm^{-2} was demonstrated by the Si_3N_4 -modified garnet with voltage stabilized at $\sim 80 \text{ mV}$ (as further indicated by voltage profiles in the inset of Figure 4e), while the cell with bare garnet could last only 20 h with large voltage polarization of $\sim 250 \text{ mV}$.

This excellent cycling with low-voltage polarization confirms the establishment of a stable interface with low interfacial impedance by introduction of the Si_3N_4 interfacial layer. Also, longer and stable cycling with almost unchanged polarization and overpotential of $\sim 100 \text{ mV}$ was exhibited at higher current density of 0.2 mA cm^{-2} (Figure S6a,b). The prompt short circuiting of bare garnet compared to garnet with a Si_3N_4 -modified interface shows that superior stability of the interface is attained by Si_3N_4 deposition. Comparison of the performance of Si_3N_4 interlayer in this work with other reported interlayers is summarized in Table S1. It can be noticed that, for room temperature (22°C) operation, the Si_3N_4 interlayer shows remarkably low interfacial resistance at reduced voltage overpotential. Also, the critical current density of 1 mA cm^{-2} achieved is very much comparable considering the electrolyte thickness and deposition procedure employed in this work. These observations imply that Si_3N_4 coating as interlayer can homogenize current distribution at the Li/garnet interface by addressing the interface mismatch between Li-anode and SSE.

3.4. Full Cell Demonstration of Interface Stabilized SSE. Further, to demonstrate the potential to enable high-energy density Li-metal batteries by the interface stability approach developed in this work, Li/ Si_3N_4 @Al-LLZO/LFP hybrid solid-state full cells as shown in Figure 5a were assembled and tested. The cathode/garnet interface (Si_3N_4 @Al-LLZO/LFP) was wetted with a tiny amount of liquid organic electrolyte to reduce cathode/electrolyte interfacial resistance. The Li/ Si_3N_4 @Al-LLZO/LFP cells showed low charge transfer resistance (Figure S7) and stable cycling compared to Li/Al-LLZO/LFP cells (Figure S8). Figure 5b shows the galvanostatic charge/discharge cycling performance of the full cell with Si_3N_4 @Al-LLZO garnet electrolyte at current density of 0.2C . The cell delivered initial charge and discharge capacities of 146.25 and $145.11 \text{ mAh g}^{-1}$, respectively, that correspond to the Coulombic efficiency of 99.2% . The discharge capacity after 100 cycles was 130 mAh g^{-1} while maintaining the Coulombic efficiency close to 100% . As shown in Figure 5c, the full cell with Si_3N_4 @Al-LLZO garnet electrolyte exhibits well-defined and flat voltage plateaus with small polarization of $\sim 0.15 \text{ V}$ at first, 50th, and 100th

cycles tested at 0.2C and room temperature. The Si_3N_4 @Al-LLZO full cells were further cycled at various C-rates of 0.1 , 0.2 , 0.5 , and 1C . As shown in Figure 5d, the cell demonstrated good rate capability with discharge capacities of 153.8 , 142.1 , 121.7 , and 109.5 mAh g^{-1} obtained at 0.1 , 0.2 , 0.5 , and 1C , respectively. The cell displayed discharge capacity retention of 153.8 mAh g^{-1} at 0.1C which accounted for $\sim 100\%$ of the initial capacity after five cycles each of higher C-rates. These observations further validate the efficacy of introducing Si_3N_4 as Li/garnet interface modifier to obtain stable and high energy density solid-state Li-metal batteries.

4. CONCLUSIONS

The poor interfacing between Li^0 and garnet-type Al-LLZO solid-state electrolyte by introducing a sputter-coated thin Si_3N_4 intermediate layer was addressed. The Si_3N_4 coating on the Al-LLZO solid-electrolyte pellet significantly reduces Li/Al-LLZO interfacial resistance from 1197 to $84.5 \Omega \text{ cm}^2$, promotes better wettability of Li^0 with Al-LLZO electrolyte, and facilitates efficient charge transfer at the interface. Noticeably, symmetrical cells with much lower overpotential and long plating/stripping cycling for $>800 \text{ h}$ at current density of 0.1 mA cm^{-2} were demonstrated using the Si_3N_4 -modified Al-LLZO solid electrolyte. Along with it, Si_3N_4 @Al-LLZO solid electrolyte paired with Li^0 as anode and LFP as cathode exhibited stable cycling performance with excellent Coulombic efficiency compared to that for bare garnet. Introduction of Si_3N_4 facilitated formation of lithiophilic interface which in turn contributed to establishment of an intimate and conformal physical/chemical contact between garnet-type solid electrolyte and lithium. The present work successfully resolves the primary challenge of high impedance Li/garnet-type solid-electrolyte interface for solid-state batteries. These findings can provide further insights into engineered interfaces focused on development of high energy density and safe solid-state Li-metal batteries.

■ ASSOCIATED CONTENT

Supporting Information

The Supporting Information is available free of charge at <https://pubs.acs.org/doi/10.1021/acsaem.1c03157>.

Digital images of as-prepared Al-LLZO pellet; surface and cross-section SEM of pellets at different sintering temperatures; XRD and Raman showing impurity removal; EIS spectra at different temperatures; digital image of lithiation reaction; optimization of interlayer thickness; plating/stripping at 0.2 mA cm^{-2} ; Nyquist plots for full cells; full cell cycling; comparison table (PDF)

■ AUTHOR INFORMATION

Corresponding Author

Quinn Qiao — Mechanical and Aerospace Engineering, Syracuse University, Syracuse, New York 13244, United States; orcid.org/0000-0002-4555-7887; Email: quqiao@syr.edu

Authors

Abiral Baniya — Mechanical and Aerospace Engineering, Syracuse University, Syracuse, New York 13244, United States; orcid.org/0000-0002-7341-0022

Ashim Gurung – Department of Electrical Engineering and Computer Science, South Dakota State University, Brookings, South Dakota 57007, United States

Jyotshna Pokharel – Department of Electrical Engineering and Computer Science, South Dakota State University, Brookings, South Dakota 57007, United States

Ke Chen – Department of Electrical Engineering and Computer Science, South Dakota State University, Brookings, South Dakota 57007, United States; orcid.org/0000-0003-3511-3112

Rajesh Pathak – Applied Materials Division, Argonne National Laboratory, Lemont, Illinois 60439, United States

Buddhi Sagar Lamsal – Department of Electrical Engineering and Computer Science, South Dakota State University, Brookings, South Dakota 57007, United States

Nabin Ghimire – Department of Electrical Engineering and Computer Science, South Dakota State University, Brookings, South Dakota 57007, United States; orcid.org/0000-0003-4016-2744

Raja Sekhar Bobba – Mechanical and Aerospace Engineering, Syracuse University, Syracuse, New York 13244, United States

Sheikh Ifatur Rahman – Department of Electrical Engineering and Computer Science, South Dakota State University, Brookings, South Dakota 57007, United States; orcid.org/0000-0002-9809-5102

Sally Mabrouk – Mechanical and Aerospace Engineering, Syracuse University, Syracuse, New York 13244, United States

Alevtina L. Smirnova – Department of Chemistry and Applied Biological Sciences, South Dakota School of Mines and Technology, Rapid City, South Dakota 57701, United States; orcid.org/0000-0003-1520-0331

Kang Xu – Battery Science Branch, Sensor and Electron Devices Directorate, U.S. Army Research Laboratory, Adelphi, Maryland 20783, United States

Complete contact information is available at:

<https://pubs.acs.org/10.1021/acsaem.1c03157>

Notes

The authors declare no competing financial interest.

ACKNOWLEDGMENTS

This work has been financially supported by Syracuse University and NSF IUCRC Center for Solid-State Electric Power Storage (CEPS) grant (2052611).

REFERENCES

- (1) Armand, M.; Tarascon, J.-M. Building better batteries. *nature* **2008**, *451* (7179), 652.
- (2) Peng, L.; Zhu, Y.; Chen, D.; Ruoff, R. S.; Yu, G. Two-Dimensional Materials for Beyond-Lithium-Ion Batteries. *Adv. Energy Mater.* **2016**, *6* (11), 1600025.
- (3) Xu, W.; Wang, J.; Ding, F.; Chen, X.; Nasybulin, E.; Zhang, Y.; Zhang, J.-G. Lithium metal anodes for rechargeable batteries. *Energy Environ. Sci.* **2014**, *7* (2), 513–537.
- (4) Dunn, B.; Kamath, H.; Tarascon, J.-M. Electrical energy storage for the grid: a battery of choices. *Science* **2011**, *334* (6058), 928–935.
- (5) Hu, Y.-S. Batteries: Getting solid. *Nat. Energy* **2016**, *1* (4), 16042.
- (6) Janek, J.; Zeier, W. G. A solid future for battery development. *Nat. Energy* **2016**, *1* (9), 16141.
- (7) Ma, C.; Chen, K.; Liang, C.; Nan, C.-W.; Ishikawa, R.; More, K.; Chi, M. Atomic-scale origin of the large grain-boundary resistance in

perovskite Li-ion-conducting solid electrolytes. *Energy Environ. Sci.* **2014**, *7* (5), 1638–1642.

(8) Dondelinger, M.; Swanson, J.; Nasymov, G.; Jahnke, C.; Qiao, Q.; Wu, J.; Widener, C.; Numan-Al-Mobin, A. M.; Smirnova, A. Electrochemical stability of lithium halide electrolyte with antiperovskite crystal structure. *Electrochim. Acta* **2019**, *306*, 498–505.

(9) Hong, H.-P. Crystal structure and ionic conductivity of Li₁₄Zn (GeO₄)₄ and other new Li⁺ superionic conductors. *Mater. Res. Bull.* **1978**, *13* (2), 117–124.

(10) Kanno, R.; Hata, T.; Kawamoto, Y.; Irie, M. Synthesis of a new lithium ionic conductor, thio-LISICON–lithium germanium sulfide system. *Solid State Ionics* **2000**, *130* (1–2), 97–104.

(11) Monchak, M.; Hupfer, T.; Senyshyn, A.; Boysen, H.; Chernyshov, D.; Hansen, T.; Schell, K. G.; Bucharsky, E. C.; Hoffmann, M. J.; Ehrenberg, H. Lithium diffusion pathway in Li_{1.3}Al_{0.3}Ti_{1.7}(PO₄)₃ (LATP) superionic conductor. *Inorganic Chemistry* **2016**, *55* (6), 2941–2945.

(12) Murugan, R.; Thangadurai, V.; Weppner, W. Fast lithium ion conduction in garnet-type Li₇La₃Zr₂O₁₂. *Angew. Chem., Int. Ed.* **2007**, *46* (41), 7778–7781.

(13) Bron, P.; Johansson, S.; Zick, K.; Schmedt auf der Gunne, J.; Dehnen, S.; Roling, B. Li₁₀SnP₂S₁₂: An affordable lithium superionic conductor. *J. Am. Chem. Soc.* **2013**, *135* (42), 15694–15697.

(14) Deiseroth, H. J.; Kong, S. T.; Eckert, H.; Vannahme, J.; Reiner, C.; Zaiß, T.; Schlosser, M. Li₆PS₅X: a class of crystalline Li-rich solids with an unusually high Li⁺ mobility. *Angew. Chem., Int. Ed.* **2008**, *47* (4), 755–758.

(15) Kamaya, N.; Homma, K.; Yamakawa, Y.; Hirayama, M.; Kanno, R.; Yonemura, M.; Kamiyama, T.; Kato, Y.; Hama, S.; Kawamoto, K.; et al. A lithium superionic conductor. *Nat. Mater.* **2011**, *10* (9), 682–686.

(16) Li, Y.; Zhou, W.; Chen, X.; Lü, X.; Cui, Z.; Xin, S.; Xue, L.; Jia, Q.; Goodenough, J. B. Mastering the interface for advanced all-solid-state lithium rechargeable batteries. *Proc. Natl. Acad. Sci. U. S. A.* **2016**, *113* (47), 13313–13317.

(17) Wenzel, S.; Leichtweiss, T.; Krüger, D.; Sann, J.; Janek, J. Interphase formation on lithium solid electrolytes—An in situ approach to study interfacial reactions by photoelectron spectroscopy. *Solid State Ionics* **2015**, *278*, 98–105.

(18) Zhu, Y.; He, X.; Mo, Y. Origin of outstanding stability in the lithium solid electrolyte materials: insights from thermodynamic analyses based on first-principles calculations. *ACS Appl. Mater. Interfaces* **2015**, *7* (42), 23685–23693.

(19) Zhu, Y.; He, X.; Mo, Y. First principles study on electrochemical and chemical stability of solid electrolyte–electrode interfaces in all-solid-state Li-ion batteries. *Journal of Materials Chemistry A* **2016**, *4* (9), 3253–3266.

(20) Bates, J. B.; Dudney, N. J.; Gruzalski, G. R.; Zuhr, R. A.; Choudhury, A.; Luck, C. F.; Robertson, J. D. Electrical properties of amorphous lithium electrolyte thin films. *Solid State Ionics* **1992**, *53–56*, 647–654.

(21) Bates, J. B.; Dudney, N. J.; Lubben, D. C.; Gruzalski, G. R.; Kwak, B. S.; Yu, X.; Zuhr, R. A. Thin-film rechargeable lithium batteries. *J. Power Sour.* **1995**, *54* (1), 58–62.

(22) Aono, H.; Sugimoto, E.; Sadaoka, Y.; Imanaka, N.; Adachi, G. y. Ionic conductivity of solid electrolytes based on lithium titanium phosphate. *J. Electrochem. Soc.* **1990**, *137* (4), 1023–1027.

(23) Ding, Z.; Li, J.; Li, J.; An, C. Interfaces: Key issue to be solved for all solid-state lithium battery technologies. *J. Electrochem. Soc.* **2020**, *167* (7), 070541.

(24) Liu, Q.; Geng, Z.; Han, C.; Fu, Y.; Li, S.; He, Y.-b.; Kang, F.; Li, B. Challenges and perspectives of garnet solid electrolytes for all solid-state lithium batteries. *J. Power Sources* **2018**, *389*, 120–134.

(25) Zhang, X.; Liu, T.; Zhang, S.; Huang, X.; Xu, B.; Lin, Y.; Xu, B.; Li, L.; Nan, C.-W.; Shen, Y. Synergistic coupling between Li₆75La₃Zr_{1.75}Ta_{0.25}O₁₂ and poly (vinylidene fluoride) induces high ionic conductivity, mechanical strength, and thermal stability of solid composite electrolytes. *J. Am. Chem. Soc.* **2017**, *139* (39), 13779–13785.

(26) Gurung, A.; Pokharel, J.; Baniya, A.; Pathak, R.; Chen, K.; Lamsal, B. S.; Ghimire, N.; Zhang, W.-H.; Zhou, Y.; Qiao, Q. A review on strategies addressing interface incompatibilities in inorganic all-solid-state lithium batteries. *Sustainable Energy & Fuels* **2019**, *3* (12), 3279–3309.

(27) Li, Y.; Xu, B.; Xu, H.; Duan, H.; Lü, X.; Xin, S.; Zhou, W.; Xue, L.; Fu, G.; Manthiram, A.; et al. Hybrid polymer/garnet electrolyte with a small interfacial resistance for lithium-ion batteries. *Angew. Chem., Int. Ed.* **2017**, *56* (3), 753–756.

(28) Cheng, L.; Crumlin, E. J.; Chen, W.; Qiao, R.; Hou, H.; Lux, S. F.; Zorba, V.; Russo, R.; Kostecki, R.; Liu, Z.; et al. The origin of high electrolyte–electrode interfacial resistances in lithium cells containing garnet type solid electrolytes. *Phys. Chem. Chem. Phys.* **2014**, *16* (34), 18294–18300.

(29) Sharafi, A.; Kazyak, E.; Davis, A. L.; Yu, S.; Thompson, T.; Siegel, D. J.; Dasgupta, N. P.; Sakamoto, J. Surface chemistry mechanism of ultra-low interfacial resistance in the solid-state electrolyte $\text{Li}_7\text{La}_3\text{Zr}_2\text{O}_{12}$. *Chem. Mater.* **2017**, *29* (18), 7961–7968.

(30) Tsai, C.-L.; Roddatis, V.; Chandran, C. V.; Ma, Q.; Uhlenbruck, S.; Bram, M.; Heitjans, P.; Guillon, O. $\text{Li}_7\text{La}_3\text{Zr}_2\text{O}_{12}$ interface modification for Li dendrite prevention. *ACS Appl. Mater. Interfaces* **2016**, *8* (16), 10617–10626.

(31) Wakasugi, J.; Munakata, H.; Kanamura, K. Effect of gold layer on interface resistance between lithium metal anode and $\text{Li}_6.25\text{Al}_0.25\text{La}_3\text{Zr}_2\text{O}_{12}$ solid electrolyte. *J. Electrochem. Soc.* **2017**, *164* (6), A1022.

(32) Fu, K. K.; Gong, Y.; Liu, B.; Zhu, Y.; Xu, S.; Yao, Y.; Luo, W.; Wang, C.; Lacey, S. D.; Dai, J.; et al. Toward garnet electrolyte-based Li metal batteries: An ultrathin, highly effective, artificial solid-state electrolyte/metallic Li interface. *Sci. Adv.* **2017**, *3* (4), e1601659.

(33) Luo, W.; Gong, Y.; Zhu, Y.; Fu, K. K.; Dai, J.; Lacey, S. D.; Wang, C.; Liu, B.; Han, X.; Mo, Y.; et al. Transition from superlithiophobicity to superlithiophilicity of garnet solid-state electrolyte. *J. Am. Chem. Soc.* **2016**, *138* (37), 12258–12262.

(34) Luo, W.; Gong, Y.; Zhu, Y.; Li, Y.; Yao, Y.; Zhang, Y.; Fu, K.; Pastel, G.; Lin, C. F.; Mo, Y.; et al. Reducing interfacial resistance between garnet-structured solid-state electrolyte and Li-metal anode by a germanium layer. *Adv. Mater.* **2017**, *29* (22), 1606042.

(35) Fu, K.; Gong, Y.; Fu, Z.; Xie, H.; Yao, Y.; Liu, B.; Carter, M.; Wachsman, E.; Hu, L. Transient behavior of the metal interface in lithium metal–garnet batteries. *Angew. Chem., Int. Ed.* **2017**, *56* (47), 14942–14947.

(36) Han, X.; Gong, Y.; Fu, K. K.; He, X.; Hitz, G. T.; Dai, J.; Pearse, A.; Liu, B.; Wang, H.; Rubloff, G.; et al. Negating interfacial impedance in garnet-based solid-state Li metal batteries. *Nat. Mater.* **2017**, *16* (5), 572–579.

(37) Wang, C.; Gong, Y.; Liu, B.; Fu, K.; Yao, Y.; Hitz, E.; Li, Y.; Dai, J.; Xu, S.; Luo, W.; et al. Conformal, nanoscale ZnO surface modification of garnet-based solid-state electrolyte for lithium metal anodes. *Nano Lett.* **2017**, *17* (1), 565–571.

(38) Shao, Y.; Wang, H.; Gong, Z.; Wang, D.; Zheng, B.; Zhu, J.; Lu, Y.; Hu, Y.-S.; Guo, X.; Li, H.; et al. Drawing a soft interface: An effective interfacial modification strategy for garnet-type solid-state Li batteries. *ACS Energy Lett.* **2018**, *3* (6), 1212–1218.

(39) Zhu, Y.; He, X.; Mo, Y. Strategies based on nitride materials chemistry to stabilize Li metal anode. *Advanced Science* **2017**, *4* (8), 1600517.

(40) Xue, W.; Yang, Y.; Yang, Q.; Liu, Y.; Wang, L.; Chen, C.; Cheng, R. The effect of sintering process on lithium ionic conductivity of $\text{Li}_{6.4}\text{Al}_{0.2}\text{La}_3\text{Zr}_2\text{O}_{12}$ garnet produced by solid-state synthesis. *RSC Adv.* **2018**, *8* (24), 13083–13088.

(41) Allen, J. L.; Wolfenstine, J.; Rangasamy, E.; Sakamoto, J. Effect of substitution (Ta, Al, Ga) on the conductivity of $\text{Li}_7\text{La}_3\text{Zr}_2\text{O}_{12}$. *J. Power Sources* **2012**, *206*, 315–319.

(42) Rangasamy, E.; Wolfenstine, J.; Sakamoto, J. The role of Al and Li concentration on the formation of cubic garnet solid electrolyte of nominal composition $\text{Li}_7\text{La}_3\text{Zr}_2\text{O}_{12}$. *Solid State Ionics* **2012**, *206*, 28–32.

(43) Shimonishi, Y.; Toda, A.; Zhang, T.; Hirano, A.; Imanishi, N.; Yamamoto, O.; Takeda, Y. Synthesis of garnet-type $\text{Li}_{7-x}\text{La}_3\text{Zr}_2\text{O}_{12-1/2x}$ and its stability in aqueous solutions. *Solid State Ionics* **2011**, *183* (1), 48–53.

(44) Yang, H.-C.; Hou, J.; Chen, V.; Xu, Z.-K. Surface and interface engineering for organic–inorganic composite membranes. *Journal of Materials Chemistry A* **2016**, *4* (25), 9716–9729.

(45) Cheng, X. B.; Hou, T. Z.; Zhang, R.; Peng, H. J.; Zhao, C. Z.; Huang, J. Q.; Zhang, Q. Dendrite-free lithium deposition induced by uniformly distributed lithium ions for efficient lithium metal batteries. *Advanced materials* **2016**, *28* (15), 2888–2895.

(46) Xiang, J.; Yuan, L.; Shen, Y.; Cheng, Z.; Yuan, K.; Guo, Z.; Zhang, Y.; Chen, X.; Huang, Y. Improved Rechargeability of Lithium Metal Anode via Controlling Lithium-Ion Flux. *Adv. Energy Mater.* **2018**, *8* (36), 1802352.

(47) Guo, Y.; Ouyang, Y.; Li, D.; Wei, Y.; Zhai, T.; Li, H. PMMA-assisted Li deposition towards 3D continuous dendrite-free lithium anode. *Energy Storage Materials* **2019**, *16*, 203–211.

(48) Guan, X.; Wang, A.; Liu, S.; Li, G.; Liang, F.; Yang, Y. W.; Liu, X.; Luo, J. Controlling nucleation in lithium metal anodes. *Small* **2018**, *14* (37), 1801423.

(49) Liu, Y.; Lin, D.; Yuen, P. Y.; Liu, K.; Xie, J.; Dauskardt, R. H.; Cui, Y. An artificial solid electrolyte interphase with high Li-ion conductivity, mechanical strength, and flexibility for stable lithium metal anodes. *Adv. Mater.* **2017**, *29* (10), 1605531.

(50) Li, X.; Kersey-Bronec, F. E.; Ke, J.; Cloud, J. E.; Wang, Y.; Ngo, C.; Pylypenko, S.; Yang, Y. Study of lithium silicide nanoparticles as anode materials for advanced lithium ion batteries. *ACS Appl. Mater. Interfaces* **2017**, *9* (19), 16071–16080.

(51) Lang, J.; Charlot, J. $\text{Li}_3\text{N}-\text{Si}_3\text{N}_4$ system. *Rev. Chim. Miner.* **1970**, *7* (1), 121–131.

(52) Yamane, H.; Kikkawa, S.; Koizumi, M. Preparation of lithium silicon nitrides and their lithium ion conductivity. *Solid State Ionics* **1987**, *25* (2–3), 183–191.

(53) Ulvestad, A.; Mæhlen, J. P.; Kirkengen, M. Silicon nitride as anode material for Li-ion batteries: Understanding the SiN_x conversion reaction. *J. Power Sources* **2018**, *399*, 414–421.

(54) Li, Y.; Hirosaki, N.; Xie, R.; Takeka, T.; Mitomo, M. Crystal, electronic structures and photoluminescence properties of rare-earth doped LiSi_2N_3 . *J. Solid State Chem.* **2009**, *182* (2), 301–311.

(55) Houmes, J. D.; zur Loyer, H.-C. Microwave synthesis of ternary nitride materials. *J. Solid State Chem.* **1997**, *130* (2), 266–271.

(56) Wen, Z.; Wang, K.; Chen, L.; Xie, J. A new ternary composite lithium silicon nitride as anode material for lithium ion batteries. *Electrochemistry communications* **2006**, *8* (8), 1349–1352.

(57) Hashim, U.; Chong, S.W.; Liu, W.-W. Fabrication of silicon nitride ion sensitive field-effect transistor for pH measurement and DNA immobilization/hybridization. *J. Nanomater.* **2013**, *2013*, No. 542737.

(58) Zeuner, M.; Pagano, S.; Schnick, W. Nitridosilicates and oxonitridosilicates: from ceramic materials to structural and functional diversity. *Angew. Chem., Int. Ed.* **2011**, *50* (34), 7754–7775.

(59) Raghavan, R. Synthesis and electrochemical characterization of Silicon clathrates as anode materials for Lithium ion batteries. M.S. Thesis, Arizona State University, 2013.

(60) Yamashita, T.; Kuwano, S.; Kuriyama, K.; Kushida, K. Optical band gap of Li_8SiN_4 with disordered structure as a cathode material of lithium secondary batteries. *physica status solidi (c)* **2015**, *12* (6), 845–848.

(61) Xu, H.; Li, Y.; Zhou, A.; Wu, N.; Xin, S.; Li, Z.; Goodenough, J. B. Li_3N -Modified garnet electrolyte for all-solid-state lithium metal batteries operated at 40°C . *Nano Lett.* **2018**, *18* (11), 7414–7418.

(62) Chen, K.; Pathak, R.; Gurung, A.; Adhamash, E. A.; Bahrami, B.; He, Q.; Qiao, H.; Smirnova, A. L.; Wu, J. J.; Qiao, Q.; et al. Flower-shaped lithium nitride as a protective layer via facile plasma activation for stable lithium metal anodes. *Energy Storage Mater.* **2019**, *18*, 389–396.

(63) Takeda, Y.; Yamamoto, O.; Imanishi, N. Lithium dendrite formation on a lithium metal anode from liquid, polymer and solid electrolytes. *Electrochemistry* 2016, 84 (4), 210–218.